Zinc Speciation in a Contaminated Aquatic Environment: Characterization of Environmental Particles by Analytical Electron Microscopy

ARTICLE *in* ENVIRONMENTAL SCIENCE AND TECHNOLOGY · APRIL 2000

Impact Factor: 5.33 · DOI: 10.1021/es991167z

3 AUTHORS, INCLUDING:

Samuel M. Webb
Stanford University
136 PUBLICATIONS **3,710** CITATIONS

Environ. Sci. Technol. **2000**, *34,* 1926−1933

Zinc Speciation in a Contaminated Aquatic Environment: Characterization of Environmental Particles by Analytical Electron Microscopy

SAMUEL M. WEBB,[†] GARY G. LEPPARD,[‡] AND JEAN-FRANÇOIS GAILLARD*,[†]

Department of Civil Engineering, Northwestern University, 2145 Sheridan Road, Evanston, Illinois 60208-3109, and National Water Research Institute, Environment Canada, Burlington, ONT L7R 4A6, Canada

Analytical electron microscopy (AEM) was used to characterize individual aquatic particles in a lake that has been contaminated by zinc smelting operations. Samples were collected from the sediments and the water column of the lake along a gradient of metal contamination. The samples were prepared to preserve their aqueous nature, and thin sections were observed by transmission electron microscopy (TEM). Zinc bearing particles were characterized by different morphologies ranging from near spherical large colloids (i.e., a few 100 nm) to small grains either intimately associated with biological templates or present as separate amorphous entities. Elemental associations were determined for each individual particle by X-ray energy dispersive spectrometry (EDS). These analyses revealed the pervasive presence of Zn through the aquatic environment and its intimate combination with Fe and P in biotic structures. The association of Zn and P was most prevalent close to the source of contamination, whereas afar Zn was primarily found in sulfur moieties. Cluster analyses, performed on four different sets of EDS measurements, exemplify the fate of Zn in the lake by quantifying changes in elemental associations.

Introduction

Industrial activities based on metal smelting operations have introduced large concentrations of metals in aquatic systems *(1)*. The design of appropriate cleanup actions rests on the detailed characterization of the fate of metals in the aqueous environment, so that educated choices can be made, e.g., dredging and disposal or "intrinsic remediation". For this purpose, one needs to assess the mobility, the reactivity, and the toxicity of these contaminants in the impacted environment. Consequently, the determination of the chemical speciation of metals becomes a key issue. Often, this is achieved by performing thermodynamic calculations, coupled to an appropriate surface complexation model, relying on the analyses of the total dissolved metal concentration and estimates of adsorption sites *(2, 3)*. However, this approach can be misleading because natural systems are quite frequently out of equilibrium *(4)*, and because biological systems have evolved a variety of mechanisms to respond to metal stress, some of which involve a respeciation of the metals *(5−9)*. Therefore, the alternative consists of determining analytically the speciation of the elements of interest.

Organic and inorganic particles that are present in aquatic systems (i.e., humics, polysaccharides, microorganisms, iron and manganese oxides and oxyhydroxides, and clays) have been reported to mediate the cycling of both essential and toxic trace metals *(10−14)*. Metal−mineral associations have been documented primarily using chemical extractions that were based on wet methods *(15−17)*. These protocols, however, have been questioned *(18−20)* because metals can redistribute to other remaining phases during the sequential extractions, and the target phases may not be the only reactive entities. In addition, they are bulk techniques, and they do not establish chemical speciation on an individual particle basis, as may be relevant when dealing with biological related materials.

Transmission electron microscopy (TEM), coupled with energy dispersive spectroscopy (EDS), has been shown to be an extremely powerful tool for examining geochemical questions on the individual particle scale. In particular, TEM-EDS is well suited to provide information on the size, morphology, crystallinity, and elemental composition of single particles as well as on their physical and spatial associations *(21, 22)*. Recent studies have used TEM-EDS to examine mineral associations in aquifers *(23)*, heavy metal sulfide precipitation in soils *(24)*, chemical speciation of metals in lakes *(25, 26)*, and immobilization of dissolved metals onto minerals and biomass *(27−29)* as well as weathering and diagenetic reactions in lake sediments *(30, 31)*.

However, the classical procedures of specimen preparation for TEM observations often lead to artifacts produced through the dehydration process. These artifacts may be quite substantial and include effects such as shrinkage and aggregation of particles *(32)*. To avoid these methodological problems, a technique which utilizes an hydrophilic resin to embed the sample *(33−35)* has been used to fix the specimens in their native positions with their natural associations intact. The Nanoplast resin has been shown to provide the optimal qualities for embedding organic and mineral material in aquatic matrices *(34−37)*.

This study aims to examine directly the intimate associations of zinc in contaminated sediments and aquatic particles at the individual particle scale and, in particular, to observe the influence that biological processes have on the distribution of zinc in the system. In addition to identifying the major morphologies of particles in which zinc is present, the elemental associations of important particles will be examined. These observations are important to make directly, as many of the insights that they may give might be missed when making inferences from bulk chemical data.

Methods and Materials

Site Characterization. Lake DePue is a moderately sized (ca. 524 acres) backwater lake of the Illinois River located in central, northern Illinois, about 20 km west of LaSalle and 170 km west of Chicago. Land use in the region is primarily agricultural. Lake DePue is connected to the Illinois River by a narrow channel at the west end of the lake. The lake is very shallow in the summer months, with a maximum depth of approximately 2 m in July of 1998. Shallow parts of the lake, especially at the northwest and east end, consist of wide, marshy areas. The water during the sampling period was

* Corresponding author phone: (847)467-1376; fax: (847)491-4011; e-mail: jf-gaillard@nwu.edu.
[†] Northwestern University.
[‡] National Water Research Institute, Environment Canada.

10.1021/es991167z CCC: $19.00

Published on Web 04/12/2000

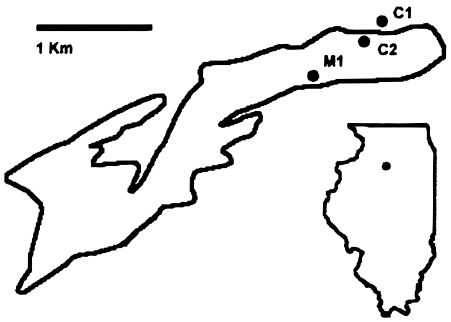

FIGURE 1. Location of sampling sites in Lake DePue, IL. Inset shows location of DePue, IL, approximately 170 km west of Chicago, IL.

extremely turbid with a high concentration of suspended solids. Industrial chemical operations, including zinc smelting, sulfuric acid production, and diammonium phosphate fertilizer production, have led to substantial metal and nutrient contamination of the aquatic system. The zinc smelting operations took place in DePue from 1906 to 1971. In 1967, the capacity of the plant was 71 000 tons per year *(38)*.

The sediments in the lake are composed of lightly colored particles and are generally loose, fluffy, and unconsolidated. Sedimentation rates in the lake have been reported up to 3 cm per year *(39)*. Erosion of banks, bluffs, and the adjacent and upland soils all contribute to the sediment load of the Illinois River. Poorly sorted silt and clay alluvium dominate the surficial deposits along most of the river. In addition, bluff materials also include loess and tills that have a high clay mineral content *(40)*. The fine-grained part of this sediment wash load is the principal source of sediment in backwater lakes *(41)*.

Sample Collection

Sediment and water column samples from Lake DePue were collected in September of 1998 at three collection sites (Figure 1). Each of the different sites represents a different sedimentary and contamination history environment. Core samples were collected with 60 mL syringes to piston core the top 10 cm of the sediment. Surface water samples were collected into 200 mL Nalgene bottles. All samples were stored a 4 °C during transport from the field site and were immediately processed for EM analysis at the laboratory.

Electron Microscopy

Preparation Technique. Particles were stabilized and prepared for the production of ultrathin sections for transmission electron microscopy (TEM) using procedures that minimized dehydration artifacts *(33)*. A melamine resin (Nanoplast FB101) was used as both a fixative and a hydrophilic embedding resin. This allows the preservation of extracellular structures and other colloids in their original hydrated form. The resin is prepared freshly by mixing 0.2 g of B52 catalyst (*p*-toluolsulfonic acid) to 10 g of hexamethylol-melamine-methyl ether (monomer MME7002). Aqueous samples were size fractionated through a sequential centrifugation process. Large particles in the raw surface water samples were removed by allowing the sample to gravitationally settle for 2.5 h. The supernatant was fractionated through centrifugation at 90 g for 1 h. At each step in the sequential fractionation, the particles collected at the bottom of the tube were saved for EM analysis. Approximately 200 μL of Nanoplast resin was added to a small smear of sediment or 50 μL of fractionated particles placed on a Teflon plate. The resin-sample mixtures were placed into an oven set a 40 °C for 2 d in the presence of desiccant and, thereafter, without a desiccant at 60 °C for another 2 d. This procedure ensures optimal properties for ultrathin sectioning *(36)* with a resolution limit of approximately 1 nm. After the Nanoplast resin was cured, the sample was removed from the Teflon plate and sliced into small strips, approximately 1−2 mm thick. These slices were then placed (vertical orientation) into a BEEM capsule (type 00 large with conical tip), which was then backfilled with Spurr's epoxy resin *(42)*. The capsule with its Spurr resin was placed into a 70 °C oven for 8 h.

TABLE 1. Chemical Composition for Relevant Species in Lake DePue Water at the Various Sampling Locations

property	C_1	C_2	M_1
depth	3 cm	50 cm	200 cm
temp (°C)			27.6
D.O. (μM)			166
conductivity (μS)			0.598
pH	7.32	7.78	7.84
alkalinity	3.8/9.0 mequiv	5.3 mequiv	4.1 mequiv
$[Zn]_d$	275 ± 14 μM	298 ± 26 nM	87 ± 15 nM
$[SO_4^{2-}]$	19.4 ± 0.3 mM	563 ± 30 μM	536 ± 6 μM
$[Cl^-]$	1.09 ± 0.10 mM	1.13 ± 0.03 mM	1.15 ± 0.01 mM

After polymerization was completed, all samples were sectioned identically. Ultrathin sections for morphological and EDS analysis (75−100 nm) were obtained by sectioning with a diamond knife mounted in a RMC Ultramicrotome MT-7. These sections were then mounted on Formvar-covered copper grids. The grids were carbon-coated for stabilization in the EDS analysis. Although the Nanoplast leaves the native spatial relations of the sample intact, it is often difficult in morphological studies to visualize structures rich in organic carbon. Applying an "electron-opaque" stain to the section on grids provides differential contrast leading to more readily visible organic structures; we applied a counterstain of 1% aqueous uranyl acetate for 3 h *(33)*.

Instrumentation. Ultrathin sections of embedded samples, mounted on Formvar-coated, copper, electron microscope grids, were examined with a JEOL 1200 EXII TEMSCAN scanning-transmission electron microscope (STEM) operating at 80 keV. The characterization of particles by morphology was done with the TEM component of the STEM, which in turn allowed one to visually select specific particles or parts of particles for spectroscopy. Identification of detectable elements in mineral colloids was accomplished using energy dispersive spectrometry (EDS) microanalysis techniques. EDS was performed using the STEM equipped with a Princeton Gamma Tech Si(Li) X-ray detector in conjunction with a PGT IMIX multichannel analyzer. Analyses of element composition $Z > 10$ were made over counting periods (approximately 2 min) appropriate to collecting sufficient counts while minimizing sample decomposition. ZAF standardless analysis *(43−45)* was carried out on each of the EDS spectra using the NIST Desk Top Spectrum Analyzer and X-ray Database program *(46)*.

Results and Discussion

Sediment Characterization. The level of inorganic contaminants is the primary difference between the three sampling sites at Lake DePue. Table 1 shows the general surface water and sediment characteristics at each of the collection sites. The sediments of Lake DePue are generally characterized as loose, unconsolidated, and fine-grained silts and clays. The M_1 site is comprised of the thinnest layer of unconsolidated sediment. The stratigraphy consists of approximately 5 cm of light green-gray colored unconsolidated sediment and 15 cm of darker brown to black colored consolidated sediment. The water content of the upper, unconsolidated layer is approximately 55% and drops to 25% in the consolidated region. These layers lie on top of a clay lens that could not be penetrated by the coring device. The

core sampled from the C_2 site consisted of 80 cm of generally unconsolidated sediments, showing no significant consolidation or loss of water throughout the entire depth profile examined. The sediments are composed mainly of light green-gray silts and clays as in the upper unconsolidated sediments of M_1. At several depths (15, 22, and 33 cm), there are lenses which consist of fine sands grading to silt. These lenses also have a high content of organic plant material.

The core sample from C_1 was comprised of 50 cm of unconsolidated, watery sediment. The water content of these sediments averaged approximately 50% and reached a maximum of 70 wt %. However, the particles in this core showed more variation in their appearance and composition than at the other sampling locations. The first 6 cm of sediment are composed of green-gray silt and clays, similar to the upper sediments at the other locations. Cores from the 6−15 cm region of the core are composed of similar material but also have orange-red-ochre masses present. These pieces range from 1 mm up to 1 cm in diameter and have a maximum in number at a depth of 10−12 cm. The pieces grade to finer particles at either end of the range. The core sections from 16 to 24 cm are composed primarily of silts and clays, with pronounced lenses of organic plant detritus. Sediment stratigraphy from 24 to 38 cm is composed of finer, darker clays and silts, which contain light tan-colored clay inclusions. The inclusions are slightly more compacted than the surrounding sediment and compose up to 35% of total sediment at 32 cm depth. Adjacent to these clays is a porous gravel lens of sediment from 40 to 48 cm. The sediment contains small dark brown to black gravel grading to fine sands and containing some silt. Many of the sand grains in this region are red and orange in color. The lens contains more fine-grained particles toward the bottom and grades into mostly silts with some sands at 48 cm. The last 2 cm of the core (48−50 cm) is composed of more compacted, dark green clays.

Electron microscopy of the sediments reveals the existence of several different colloid classes present in nearly all core samples. These classes can be identified through a combination of their size, shape, electron-opacity, and elemental composition as determined by STEM-EDS. The principal constituents were bacteria, small algae, organic fibrils and matrices, clay minerals, iron hydroxides, iron−zinc phosphates, biogenic silica and diatoms, and sulfidic minerals. Carbonates, defined as particles containing primarily Mg and Ca exclusively, although found in small amounts at all collection sites, were found to be a minor component among the other major particles observed. X-ray EDS analyses showed that zinc was most prevalent on particles close to the effluent source. The details of these zinc-containing phases are discussed below.

Zinc-Bearing Particle Characterization. Distinct trends of zinc associations on colloidal particles can be observed between the various collection sites. Figure 2 (parts a and b) shows the electron micrographs, and Figure 3 (parts a and b) presents their associated EDS spectra of particles collected from the site C_1. This site is characterized by a low volume, oxic, effluent stream transporting up to 300 μM Zn over sediments that contain Zn concentrations ranging from 3% to nearly 30% by dry weight. Due to the high absolute concentration of zinc in these sediments, many of the particles from this site contain appreciable amounts of zinc. Figure 2a shows typical zinc-rich particles that range in size from 120 to 550 nm, have regular shape, and have uniform electron density. A typical EDS spectrum for these particles, shown in Figure 3a, demonstrates that they are rich in iron, zinc, and phosphorus. This morphology is the most common of the zinc bearing colloids, which often appear to be strongly associated with or entrained into biological structures. This is suggested by Figure 2b where the particles seem intimately associated with an algal cell, whose organic-rich outer surface may be acting as a template or nucleation site for particle formation. We think that the zinc in these particles could be coprecipitated or coentrained, as such high concentrations of zinc are not likely to be present solely as a result of surface adsorption phenomena. Other zinc containing particles at this location include iron−zinc oxyhydroxides and, to a lesser degree, particles in which zinc is sorbed onto iron-rich clay minerals.

Water column particulates from the C_2 collection site were also examined. Particles examined from this locality consisted mostly of diatom frustules, clay minerals, and organic matrices. As was the case with the C_1 site, zinc was predominantly associated with iron−phosphorus rich particles. In addition to these particles, zinc was also found present at significant concentrations on iron−manganese rich precipitates on bacterial cell walls (Figures 2c and 3c). Again, these observations demonstrate the intimate relationships between biological structures (i.e. cell walls) and zinc partitioning. Additionally, these TEM observations suggest that biological surfaces are acting as templates for the formation of zinc-rich particles. Zinc was rarely detected on any of the clay minerals present in the water column of the lake and was never measured above detection limits in diatom frustules or biogenic silica particles represented by frustule fragments (Figures 2d and 3d).

Figures 2e and 3e show the micrograph and EDS spectrum of sediment collected in the lake at the outlet of the effluent creek (C_2). The sediments in the lake become anaerobic very rapidly, in contrast to the more oxic sediments at C_1. The zinc contamination in this region of the lake is still significant but much smaller than at C_1. Sediment zinc concentrations range from 1% to 5% by dry weight. Particles containing measurable concentrations of zinc in C_2 sediments fall into a much narrower type classification than at C_1. The most common particulate form of zinc is shown in Figure 2e. These are small, rounded globules, typically 45−210 nm (average 82 nm) in diameter, that appear to consistently have poorly defined edges and extremely irregular electron density, suggestive of an amorphous nature. The zinc in these particles is nearly always present with a large concentration of sulfur. This suggests that there is diagenetic formation of ZnS in the sediments at this location. In addition to these globules, zinc is also present in a significant fraction in mineralized layers. EDS spectra from these mineralized materials show also strong zinc and sulfur contributions.

Sediments were also collected from a mid-lake site (M_1), which has a much lower level of zinc contamination. Typical zinc concentrations at this location range from a background level of 50 ppm to 0.5% by dry weight. Consequently, zinc is found to be abundant in relatively few particles as detected by EDS. Particles in this region consisted mostly of biogenic silica, clay minerals, and bacterial cells. At this site, zinc was primarily found to be associated with sulfur.

Quantitative Results. The average elemental composition of each of the major particle classifications for each sampling location is presented in Table 2. Note that these are the percent compositions, on a mole basis, of the elements measured within the analytical window of the EDS detector. Since a Be window was used, these compositions do not include the concentration of lighter elements such as C, N, and O. Several conclusions emerge from these data. First, the major element composition (i.e., Si, Al, Mg, K) of the clay particle classification remains nearly the same at all three sampling locations. This is not surprising, since the clay particles are likely derived from the same Quaternary glacial sedimentary sources in the region. Second, based on the overall average elemental composition for the clay mineral morphology, the clays consist of a mixture of illite, chlorite, and kaolinite *(47)*, and zinc concentrations present on these

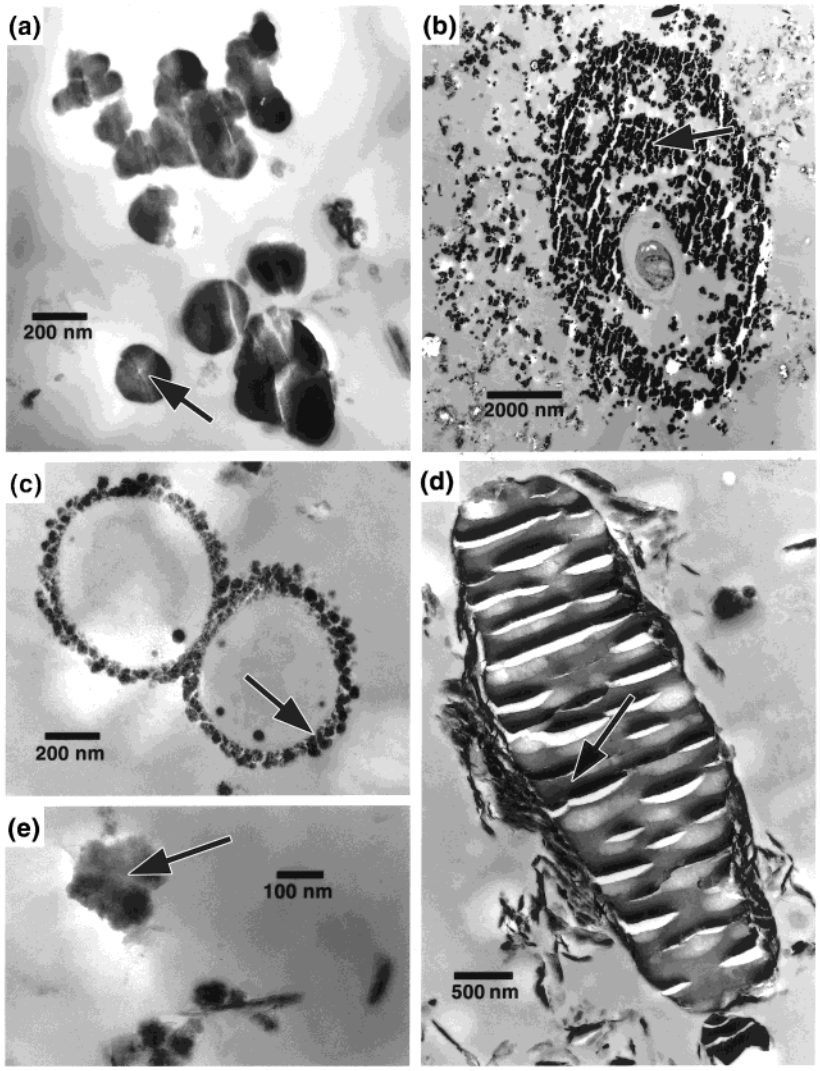

FIGURE 2. TEM micrographs of particles imaged from Lake DePue. The images shown are representative of key features in the lake and are a subset of over 250 observations. The arrow in each picture shows where the EDS spectrum was collected (see Figure 3). (a) Well crystalline, regular shaped globules found in the creek sediments (C_1) of Lake DePue. The particles are noted to have a uniform electron density and have very well-defined edges. The globules are the dominant morphology of zinc containing particles in this region. (b) Algal cell (center) surrounded by a large number of zinc containing particles at site C_1. Biological membranes in this micrograph were enhanced with a uranyl acetate stain. (c) Bacterial cells in the water column collected at site C_2. The electron density of the precipitate at the bacterial wall is due to the presence metals. Bacteria and other similar biological structures are the principal morphology of zinc containing particles in the water column of the lake. (d) Diatom frustule found in the water column of Lake DePue at C_2. (e) Globules collected from sediments at the creek outlet (C_2) which show irregular electron density, suggesting an amorphous nature.

particles decrease from C_1 to C_2 to M_1 as expected by the drop in the contaminant levels between these sites. The presence of zinc is this carrier phase is likely due to sorption processes either onto clay minerals or onto iron oxide coatings precipitated on the clays. We can also notice here that there is no obvious correlation between Zn and Fe concentrations in this clay particle category. Last, a similar trend in zinc concentration is also seen in the organic material. In this context, the organic material consists of bacterial cells, microalgae, capsular layers, and fibrils. Again, the zinc present in this material is due certainly due the presence of specific metal binding sites, and the amount of zinc decreases as the level of contamination decreases.

Analytical EDS provides estimates of the elemental ratios of the major zinc bearing phases found in Lake DePue. The analyses of the globules rich in Fe, P, and Zn, found in the C_1 sediments show that the amount of phosphorus present remains relatively consistent since P accounts for 63% ± 5% of the elements measured within each spectrum (as explained before, this composition does not include light elements such as C, N, and O). In contrast, the distribution of iron and zinc in these particles is much more variable, although the sum of the relative concentrations of these two elements is quite constant, typically 24% ± 4%. The concentrations of iron and zinc, however, are anticorrelated. A plot of Fe vs Zn shows a slope of -1.08 ± 0.12 with a correlation coefficient of 0.704. This suggests that zinc and iron are substituting for each other within the matrix of these particles. Globules in the water column of C_2 are slightly different in nature. They show a more consistent concentration of Fe, and they contain proportionally more phosphate (P 57% ± 5.3%, Fe 7.0% ± 0.8%; Zn 2.2% ± 0.8%). At this location, cation substitution does not appear to be as important as in C_1, since the relative concentration of iron remains nearly constant, whereas the fraction of zinc varies. Similar observations can be made for the zinc and sulfur rich particles in the sediments at C_2 and M_1. Since the particles were sampled from the anaerobic zone of the sediments, the dominant form of sulfur bound with zinc or iron is likely to be sulfide. The average elemental ratios measured at these two sites were Zn:S = 1:4 at C_2 and

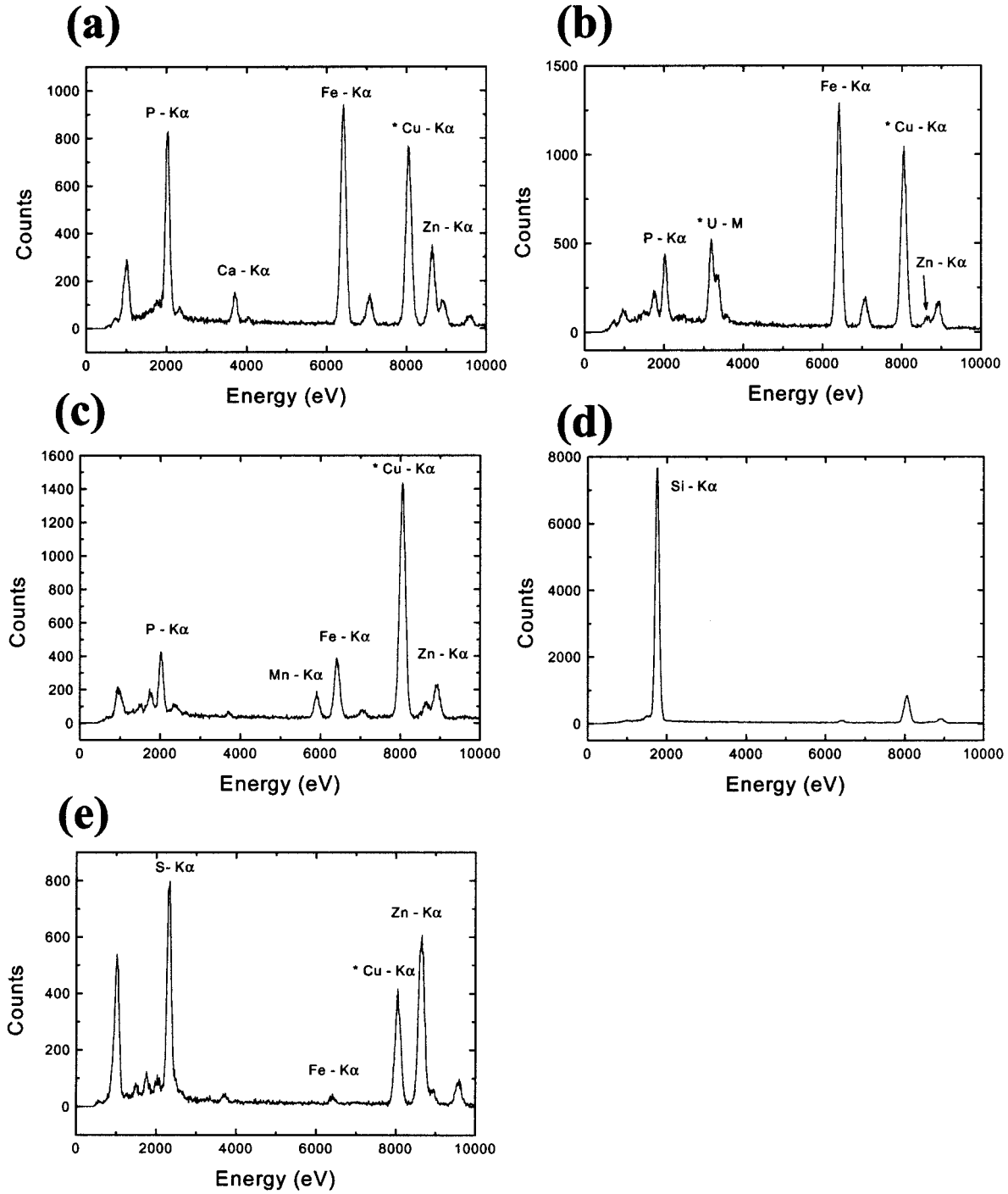

FIGURE 3. EDS spectra collected from the particles shown in Figure 2. Peaks labeled with an asterisk are contaminant peaks. (a) Well crystalline globules from C_1 are composed primarily of iron−zinc-phosphates. These particle associations are ubiquitous throughout the C_1 sediments and C_2 water column. The contaminant peak from Cu is due to the Cu grid. (b) Particles entrained in algal associations are again composed primarily of iron−zinc-phosphates. The U peak in the spectrum is from the uranyl acetate stain used to enhance organic membranes. (c) Cell wall precipitates found on bacterial cells are composed mostly of Fe and Mn. Zinc is also found in association with these precipitates and has likely been scavenged from the water column. (d) In contrast to the biological precipitates found on microbial cell walls, diatoms, which are found in large numbers throughout the lake, do not have any zinc present in their structures within the detection limits of the EDS. The fustules are composed almost entirely of silica. (e) Amorphous particles in the anaerobic sediments show a strong association of zinc and sulfur. This is suggestive of a diagenetic formation of ZnS at depth in the sediments. The EDS spectrum shows that the particles are relatively pure, containing very little iron or other metals.

Zn:Fe:S = 1.2:0.3:3 at M_1, with Zn composing approximately 14% ± 3% of the relative particle composition.

Figure 4 shows the cluster diagrams of the major elements determined by STEM-EDS. These relations were calculated using the relative concentrations of each element, as determined by standardless ZAF analysis *(44, 46)* of the EDS measurements. The cluster diagram approach consists of a hierarchical grouping of variables, based on the similarity of their behavior. Thus, we can determine which elements are closely related to each other at each sampling location. Significant changes in zinc-bearing phases between the sampling sites can be seen in these diagrams. In the creek

TABLE 2. Average Elemental Compositions of the Major Particle Morphologies[a]

morphology	Zn	Fe	P	S	Si	Al	Na	Mg	K	Ca	Mn	Ti	Pb	Ba	Ni
							Average-C_1								
oxide clay	1.42	2.80	4.89	0.37	57.55	23.18	0.00	6.67	2.20	0.88	0.00	0.05	0.00	0.00	0.00
globule	5.66	15.45	53.62	1.83	10.14	7.46	1.54	2.79	0.00	1.51	0.00	0.00	0.00	0.00	0.00
sulfide	0.00	0.00	0.00	0.00	0.00	0.00	0.00	0.00	0.00	0.00	0.00	0.00	0.00	0.00	0.00
organic	2.21	7.90	23.79	20.62	29.57	12.26	0.00	3.31	0.00	0.32	0.00	0.00	0.00	0.00	0.00
diatom	0.16	0.20	0.00	0.00	98.34	1.29	0.00	0.00	0.00	0.00	0.00	0.00	0.00	0.00	0.00
carbonate	0.00	0.00	0.00	0.00	0.00	0.00	0.00	0.00	0.00	0.00	0.00	0.00	0.00	0.00	0.00
							Average-C_{2s}								
oxide clay	1.39	4.65	1.83	1.46	55.39	25.16	0.00	6.08	3.42	0.50	0.03	0.10	0.00	0.00	0.00
globule	0.00	0.00	0.00	0.00	0.00	0.00	0.00	0.00	0.00	0.00	0.00	0.00	0.00	0.00	0.00
sulfide	13.54	0.64	2.89	55.23	15.28	7.63	0.00	2.82	0.15	0.50	0.00	0.00	0.00	1.31	0.00
organic	2.33	7.24	2.45	4.25	55.94	21.55	0.00	5.11	0.50	0.52	0.00	0.11	0.00	0.00	0.00
diatom	0.00	0.13	0.00	0.35	98.57	0.95	0.00	0.00	0.00	0.00	0.00	0.00	0.00	0.00	0.00
carbonate	0.21	1.60	12.27	0.68	14.00	8.52	0.00	38.34	0.34	23.95	0.10	0.00	0.00	0.00	0.00
							Average-C_{2w}								
oxide clay	0.41	3.72	3.73	1.34	52.61	30.31	0.00	4.49	2.92	0.17	0.00	0.12	0.19	0.00	0.00
globule	2.06	7.32	53.72	4.09	16.34	14.73	0.00	0.63	0.04	1.07	0.00	0.00	0.00	0.00	0.00
sulfide	0.00	0.00	0.00	0.00	0.00	0.00	0.00	0.00	0.00	0.00	0.00	0.00	0.00	0.00	0.00
organic	1.83	7.33	43.90	5.16	24.45	14.48	0.00	0.00	0.06	0.85	1.94	0.00	0.00	0.00	0.00
diatom	0.06	0.19	0.50	0.00	94.57	3.94	0.00	0.00	0.30	0.13	0.05	0.27	0.00	0.00	0.00
carbonate	0.04	0.42	0.41	0.33	12.18	4.44	0.00	62.35	0.07	19.73	0.04	0.00	0.00	0.00	0.00
							Average-M_1								
oxide clay	0.16	5.13	2.74	3.20	48.06	29.45	0.00	5.71	3.12	0.17	0.00	0.09	2.03	0.00	0.13
globule	0.00	0.00	0.00	0.00	0.00	0.00	0.00	0.00	0.00	0.00	0.00	0.00	0.00	0.00	0.00
sulfide	14.17	3.87	1.05	39.65	16.42	14.86	0.00	2.25	0.00	0.80	0.00	0.00	6.93	0.00	0.00
organic	0.83	9.15	2.12	18.24	25.76	27.54	0.00	1.09	0.77	2.14	0.00	0.00	12.32	0.00	0.03
diatom	0.03	1.32	0.38	0.00	86.29	9.45	0.00	0.81	1.16	0.54	0.00	0.00	0.02	0.00	0.00
carbonate	0.01	0.66	0.00	0.44	23.83	9.48	0.00	15.75	0.28	49.28	0.00	0.16	0.00	0.00	0.11

[a] The table shows the composite average of all particles of a given morphology over all of the collection sites as well as the breakdowns of the composition at each individual site. Oxides and clay mineral have been grouped together.

sediments (C_1) zinc is associated most strongly with iron, phosphorus, and calcium. These elements are in a distinct group from the elements that compose most of the clay minerals (Si, Al, Mg, and K). In the water column of the lake, however, zinc is associated primarily with phosphorus and sulfur and to a lesser degree with iron. Again, this grouping is distinct from the clay mineral group (Si, Al, and K) and the carbonate group (Mg and Ca). The sediments in the lake (C_2 and M_1) are again significantly different from the other sampling sites. The cluster analysis shows that, at these sampling locations, zinc is associated almost exclusively with sulfur.

The iron−zinc−phosphorus particles from C_1 may have several possible origins. First, they may have originated from the industrial smelting processes and may have been transported to the lake through groundwater and surface water runoff. Second, as the concentrations of iron and zinc are relatively high in the surface waters of C_1, the particles could have formed through an abiotic, in situ precipitation. Last, these particles could have resulted from a biological process, either intracellular or extracellular, that leads to the precipitation of phosphate compounds. This last hypothesis seems to be likely since the particles appear to be intimately associated with biological cells (Figure 2b) and, in many cases, are surrounded by extracellular structures. Other biotic structures, such as intracellular polyphosphates and iron−phosphorus rich granules, have been observed directly by TEM and STEM-EDS *(48, 49)* for bacteria. In any case, our TEM observations exemplify that the distribution of zinc is inherently related to biological structures at nearly every sampling location probed. These structures not only are the dominant carriers of zinc in the lake but also may act as an important catalyst site for the formation of these particles. More work is necessary to understand the actual processes that are occurring at the level of cell walls and that are leading to the formation of the colloidal particles observed. Some pertinent results have been reported in the literature and provide some guidelines for our further studies. The fibrils (extracellular polymeric substances), which extend from the surfaces of some bacteria, possess nucleation sites for the deposition of iron and manganese oxides *(50)*. Bacterial cell walls can remove metals from dilute solutions, including simulated lake water *(51)*, and bacterial metal accumulation has been well documented in regard to cell wall interactions with metals in solution *(5, 52)*. The generation of mineralized (Ca, Si) scales and wall parts of colloidal dimensions, by internal metabolic processes in microalgae, is a phenomenon well documented, including its ultrastructural aspects *(53)*. Colloidal iron associations with surfaces of many kinds are currently being documented for suspended native particles in (iron/phosphate/organic carbon-rich) lake water *(54)*. With regard to mineral coatings on bacteria, studied *in situ* in native sediments, it has been shown recently by STEM-EDS that iron oxyhydroxide coatings on cell walls and extracellular fibrils will strongly and preferentially accumulate copper from pore water *(55)*. These works, and the present one, stress the importance of examining the microscale to elucidate important contaminant bearing phases present in aquatic ecosystems; they also stress the importance of considering biological templates as an important factor in contaminant transformations.

However, there exist some limitations inherent to this method of particle analysis. First, X-ray EDS provides only elemental concentrations. It is impossible to differentiate sulfide from sulfate for example, and some biogeochemical intuition is required to make educated guesses. Second, the EDS detector is only sensitive to relatively high elemental concentrations (greater than 0.1%). Thus, classes of particles that contained a small concentration of zinc, but that may be numerous enough to make up a significant fraction of the total particulate metal concentration, would be missed by this technique. This problem can be remedied by using complementary analytical techniques. In particular, a spectroscopic technique, such as XAS (X-ray absorption spec-

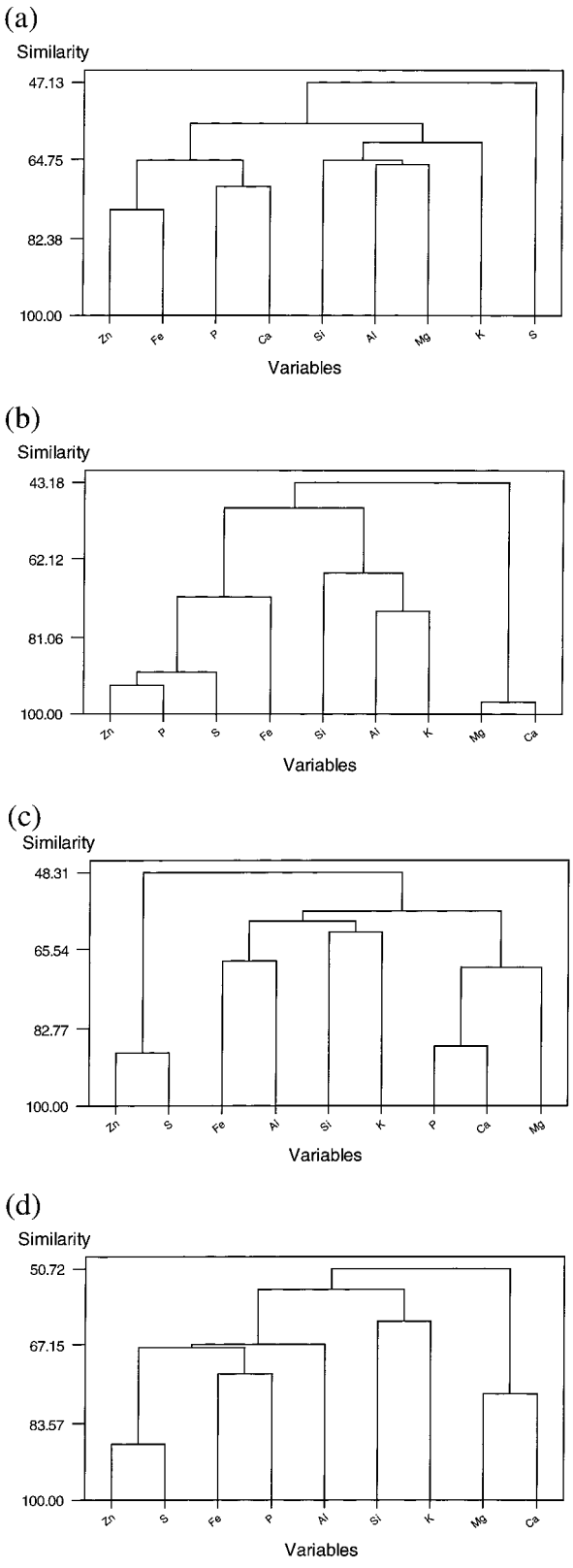

FIGURE 4. Cluster diagrams based on the ZAF corrected concentrations of each element for each of the sampling locations. The pattern of the elemental associations of zinc can be seen in these figures, from mainly zinc−iron-phosphate relationships to zinc−sulfur relationships: (a) C_1 sediment cluster diagram, which is a composite of 50 observations; (b) C_2 water column cluster diagram, a composite of 42 observations; (c) C_2 sediment cluster diagram, a composite of 34 observations; and (d) M_1 sediment cluster diagram, a composite of 28 observations.

troscopy), can be used to probe the average local coordination environment of metals *(56, 57)* and actually it proves to be quite advantageous in this case since zinc is known to be spectroscopically silent by other methods. These investigations will be reported in another paper *(58)*.

Acknowledgments

The authors would like to thank Marcia M. West for her expertise in the preparation of ultrathin-sectioned samples. Funding for this work was provided by the National Science Foundation (NSF-MCB: #9807697 to J.-F. G.) and the Illinois Department of Natural Resources (IL-DNR: #98114 to J.-F.G.).

Literature Cited

(1) Nriagu, J. O. *Environmental Impact of Smelters*; John Wiley & Sons: New York, 1984.
(2) Allison, J. D.; Brown, D. S.; Novo-Gradac, K. J. U.S. EPA: Athens, GA, 1991.
(3) Westall, J. C.; Zachara, J. L.; Morel, F. M. M. Parsons Laboratory, MIT: Cambridge, 1976.
(4) Brezonik, P. L. *Chemical Kinetics and Process Dynamics in Aquatic Systems*; Lewis: Boca Raton, 1994.
(5) *Metal Ions and Bacteria*; Beveridge, T. J., Doyle, R. J., Eds.; John Wiley: New York, 1989.
(6) Nies, D. H. *J. Bacteriol.* **1992**, *177*, 2143.
(7) Silver, S.; Phung L. T. *Annu. Rev. Microbiol.* **1996**, *50*, 753.
(8) Silver, S. *Geomicrobiology: Interactions Between Microbes and Minerals*, *Rev. Mineral.* **1997**, *35*, 345.
(9) Kushner, D. J. *Water Pollut. Res. J. Can.* **1993**, *28*, 11.
(10) Kavanaugh, M. C.; Leckie, J. O. In *Advances in Chemistry*; American Chemical Society: Washington, DC, 1980; Vol. 189.
(11) Anderson, M. A.; Rubin, A. J. *Adsorption of Inorganics at Solid−Liquid Interfaces*; Ann Arbor Science: Ann Arbor, MI, 1981.
(12) Baccini, P. In *Metal Ions in Biological Systems*; Sigel, H., Ed.; Dekker: New York, 1984; Vol. 18, pp 239−286.
(13) Salomons, W.; Förstner, U. *Metals in the Hydrocycle*; Springer: Berlin, 1984.
(14) Buffle, J. In *Ellis Horwood Series in Analytical Chemistry*; Kramer, J. R., Allen, H. E., Eds.; Horwood: Chichester, 1988.
(15) Tessier, A.; Campbell, P. G. C.; Bisson, M. *Anal. Chem.* **1979,** *51*, 844.
(16) Tessier, A.; Rapin, F.; Carignan, R. *Geochim. Cosmochim. Acta* **1985**, *49*, 183.
(17) Young, L. B.; Dutton, M.; Pick, F. R. *Biogeochemistry* **1999**, *17*, 205.
(18) Guy, R. D.; Chakrabarti, C. L.; McBain, D. C. *Water Res.* **1978**, *12*, 21.
(19) Rendell, P. S.; Batley, G. E.; Cameron, A. J. *Environ. Sci. Technol.* **1980**, *14*, 314.
(20) Tipping, E.; N. B., H.; Hilton, J.; Thompson, D. W.; Bowles, E.; Hamilton-Taylor, J. *Anal. Chem.* **1985**, *57*, 1944.
(21) Leppard, G. G.; Buffle, J.; De Vitre, R. R.; Perret, D. *Arch. Hydrobiol.* **1988**, *113*, 405.
(22) Buffle, J.; De Vitre, R.; Perret, D.; Leppard, G. G. *Geochim. Cosmochim. Acta* **1989**, *53*, 399.
(23) Swartz, C. H.; Ulery, A. L.; Gschwend, P. M. *Geochim. Cosmochim. Acta* **1997**, *61*, 707.
(24) Barnett, M. O.; Harris, L. A.; Turner, R. R.; Stevenson, R. J.; Henson, T. J.; Melton, R. C.; Hoffman, D. P. *Environ. Sci. Technol.* **1997**, *31*, 3037.
(25) Lienemann, C.-P.; Taillefert, M.; Perret, D.; Gaillard, J.-F. *Geochim. Cosmochim. Acta* **1997**, *61*, 1437.
(26) Taillefert, M.; Lienemann, C.-P.; Gaillard, J.-F.; Perret, D. *Geochim. Cosmochim. Acta* **2000**, *64*, 169.
(27) Arey, J. S.; Seaman, J. C.; Bertsch, P. M. *Environ. Sci. Technol.* **1999**, *33*, 337.
(28) Patterson, R. R.; Fendorf, S.; Fendorf, M. *Environ. Sci. Technol.* **1997**, *31*, 2039.
(29) Figueira, M. M.; Volesky, B.; Mathieu, H. J. *Environ. Sci. Technol.* **1999**, *33*, 1840.
(30) Banfield, J. F.; Jones, B. F.; Veblen, D. R. *Geochim. Cosmochim. Acta* **1991**, *55*, 2795.
(31) Banfield, J. F.; Jones, B. F.; Veblen, D. R. *Geochim. Cosmochim. Acta* **1991**, *55*, 2781.
(32) Leppard, G. G.; Burnison, B. K.; Buffle, J. *Anal. Chim. Acta* **1990**, *232*, 107.
(33) Leppard, G. G.; Heissenberger, A.; Herndl, G. J. *Mar. Ecol. Prog. Ser.* **1996**, *135*, 289.

(34) Liss, S. N.; Droppo, I. G.; Flannigan, D. T.; Leppard, G. G. *Environ. Sci. Technol.* **1996**, *30*, 680.
(35) Perret, D.; Leppard, G. G.; Muller, M.; Belzile, N.; De Vitre, R.; Buffle, J. *Water Res.* **1991**, *25*, 1333.
(36) Frösch, D.; Westphal, C. *Electron Microsc. Rev.* **1989**, *2*, 231.
(37) He, Q. H.; Leppard, G. G.; Paige, C. R.; Snodgrass, W. J. *Water Res.* **1996**, *30*, 1345.
(38) Gibb, J. P.; Cartwright, K. *Illinois State Water Survey;* Illinois State Geological Survey: Champaign, IL, 1982; p 113.
(39) Cahill, R. A.; Steele, J. D. Illinois State Geological Survey: Champaign, IL, 1986; p 61.
(40) Willman, H. B. Illinois State Geological Survey: Champaign, IL, 1973; p 48.
(41) Lee, M. T. Nanjing, China, October 1983 1984; Illinois State Water Survey Reprint 617.
(42) Spurr, A. R. *J. Ultrastruct. Res.* **1969**, *26*, 31.
(43) Reid, D. A.; Ducharme, H. C.; West, M. M.; Lott, J. N. A. *Protoplasma* **1998**, *202*, 122.
(44) Reed, S. J. B. *Electron Microprobe Analysis*, 2nd ed.; Cambridge University Press: New York, 1993.
(45) Heinrich, K. F. J. *Electron Beam X-ray Microanalysis*; Van Nostrand Reinhold: New York, 1981.
(46) Fiore, C. E.; Swyt, C. R.; Myklebust, R. L. NIST.
(47) Klein, C.; Hurlbut, C. S., Jr. *Manual of Mineralogy*, 21st ed.; John Wiley: New York, 1993.
(48) Bode, G.; Mauch, F.; Ditschuneit, H.; Malfertheiner, P. *J. Gen. Microbiol.* **1993**, *139*, 3029.
(49) Lins, U.; Farina, M. *FEMS Microbiol. Lett.* **1999**, *23*, 23.
(50) Ghiorse, W. C.; Hirsch, P. *Arch. Microbiol.* **1979**, *123*, 213.
(51) Mayers, I. T.; Beveridge, T. J. *Can. J. Microbiol.* **1989**, *35*, 764.
(52) Schultze-Lam, S.; Fortin, D.; Davis, B. S.; Beveridge, T. J. *Chem. Geol.* **1996**, *132*, 171.
(53) Dodge, J. D. *The Fine Structure of Algal Cells*; Academic Press: London, 1973.
(54) Pizarro, J.; Belzile, N.; Filella, M.; Leppard, G. G.; Negre, J.-C.; Perret, D.; Buffle, J. *Water Res.* **1995**, *29*, 617.
(55) Jackson, T. A.; West, M. M.; Leppard, G. G. *Environ. Sci. Technol.* **1999,** in press.
(56) Manceau, A.; Boisset, M.-C.; Sarret, G.; Hazemann, J.-L.; Mench, M.; Cambier, P.; Prost, R. *Environ. Sci. Technol.* **1996**, *30*, 1540.
(57) Lamoureux, M. M.; Hutton, J. C.; Styris, D. L.; Gordon, R. L. *Appl. Spectrosc.* **1995**, *49*, 808.
(58) Webb, S. M.; Gaillard, J.-F. Manuscript in preparation.

Received for review October 11, 1999. Revised manuscript received February 16, 2000. Accepted March 3, 2000.

ES991167Z